


**Pinch-off of liquid jets at the finite scale of an interface**Francisco Cruz-Mazo <sup>1,2,\*</sup> and Howard A. Stone<sup>1,†</sup><sup>1</sup>*Department of Mechanical and Aerospace Engineering,  
Princeton University, Princeton, New Jersey 08544, USA*<sup>2</sup>*Department of Ingeniería Aeroespacial y Mecánica de Fluidos, Universidad de Sevilla, 41092 Sevilla, Spain*

(Received 24 December 2020; accepted 7 January 2022; published 18 January 2022)

We derive self-similar continuum equations that govern the rupture of liquid threads at scales within the influence of interfacial dynamical effects. This regime and the obtained power-law solution for the evolution of the minimum neck radius,  $h_{\min} = 0.00107(t_b - t)^{2.34}$ , fill a void in the literature in between the classical inertial-viscous regime and the stochastic formulation and reconcile flow features such as asymptotic slow boundary conditions far away from the singularity and symmetric profiles, respectively. Due to its inherent ties to the production of monosized droplets from jetting, this work can be utilized to approach, for example, the study of electrosprays or flow focusing at these critical scales for aerospace nano-thruster technology or single-biomolecule imaging with x-ray free-electron lasers.

DOI: [10.1103/PhysRevFluids.7.L012201](https://doi.org/10.1103/PhysRevFluids.7.L012201)

The ubiquity of liquid jets in nature and their generation, stability, and controlled rupture have motivated not only fundamental research [1] but also their use in multidisciplinary endeavors in analytical chemistry [2], structural biology [3], and aerospace nanopropulsion [4] among others. Eggers [5] established the self-similar equations for the pinching process where inertia, surface tension, and viscous terms are balanced: the inertial-viscous regime (IV). The evolution of the minimum neck radius  $h_{\min}$  was found to be  $h_{\min}^{(IV)} = 0.03(\sigma/\mu)(t_b - t)$ , where  $\sigma$ ,  $\mu$ , and  $t_b$  are the surface tension, viscosity, and time of breakup, respectively. However, its range of validity is not universal as the pinch-off can be triggered upstream under a pure dominance of inertia or viscosity, although after an intermediate regime [6–8] the thread dynamics behaves according to the IV regime [5].

However, Moseler and Landman [9] demonstrated via molecular simulations how the breakup of a liquid propane jet forced through a hole with a diameter of 6 nm does not obey the exponent and predictions based on the IV analysis. To address this limitation, a stochastic force was added to the slender jet model in order to identify a regime where thermal fluctuations from the bulk can control the pinching process (the bT regime). This approach was later exploited by Eggers [10] who derived numerically  $h_{\min}^{(bT)} \propto (t_b - t)^{0.418}$ . Subsequently, researchers have studied the inclusion of vapor-pressure effects in molecular dynamic simulations [11], ultralow surface tension experiments at much larger scales [12–14], and further numerical explorations regarding the validity of the 0.418 power law for ultralow surface tension [15].

Whether the power-law exponent is determined by the balance of inertia, viscous and surface tension stresses, or stochastic forces, these works share a common assumption no matter the length scale that is under study: an interface thickness  $\delta$  such that  $\delta/h_{\min} \ll 1$ . This simplicity has a

\*fcruz5@us.es

†hastone@princeton.edu

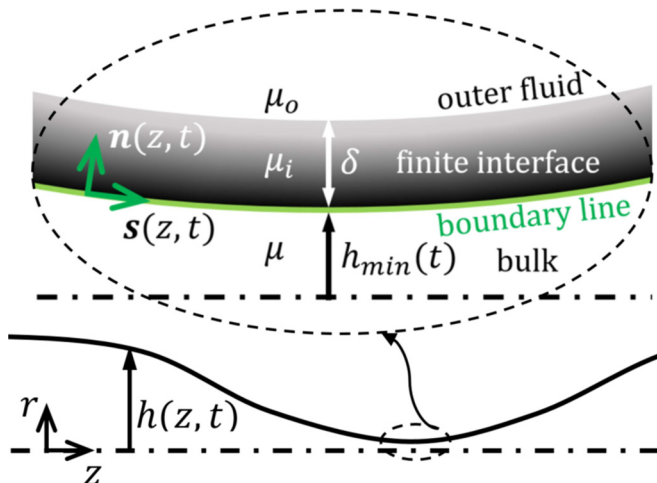


FIG. 1. Sketch about the minimum thickness of the pinching of a liquid thread. A detailed view in the vicinity of the minimum radius  $h_{\min}$  and at a scale comparable in size to the interface thickness  $\delta$  (in gray color gradient).

profound implication for the interface dynamics, which is a frozen sharp layer that affects the jet behavior through the Laplace-Young stress with a certain value for  $\sigma$ .

However, the interface cannot be considered infinitely narrow under the following scenarios: (i) during the pinch-off of jets where eventually  $\delta/h_{\min} \sim 1$  or (ii) for thin enough steady liquid jets with a radius  $h_{\infty}$  such as  $h_{\infty} \rightarrow \delta$ . It is then natural to ask: (i) does a finite interface produce intermediate spatiotemporal scales in between the IV and bT regimes? and, if so, (ii) would these novel scales lead to self-similar properties within the breakup of a liquid jet and, consequently, to a new power-law exponent for the dynamics of the minimum neck radius? In this work, we shed light on this matter by deriving an extended but analytically approachable slender model for a liquid jet that is affected by the finite thickness of the interface.

*Model formulation.* We distinguish two domains, a liquid bulk and a finite phase-graded interface, which are separated by a nonmaterial contact line as the axisymmetric surface function  $r = h(z, t)$  (Fig. 1). The classical idea [1] that we utilize is that for a sufficiently slender jet (i.e., characteristic radial  $\ell$  and axial  $L$  length scales are such as their ratio  $\epsilon = \ell/L \ll 1$ ) higher-order terms are negligible and can be removed from the set of nondimensional incompressible axisymmetric Navier-Stokes equations for the liquid bulk,

$$u_t + uu_r + vu_z = -\frac{p_r}{\epsilon^2} + \frac{u_{rr}}{\epsilon^2} + u_{zz} + \frac{u_r}{r\epsilon^2} - \frac{u}{r^2\epsilon^2}, \quad (1a)$$

$$v_t + uv_r + vv_z = -p_z + \frac{v_{rr}}{\epsilon^2} + v_{zz} + \frac{v_r}{r\epsilon^2}, \quad (1b)$$

where subscripts denote partial derivatives. The axial  $z$  and radial  $r$  lengths and time  $t$  have been, respectively, made dimensionless by the axial  $L = \mu^2/(\rho\sigma)$  and radial  $\ell = \epsilon L$  scales and the characteristic time  $\tau = \epsilon^2\mu^3/(\rho\sigma^2)$ . Note that  $p$ ,  $u$ , and  $v$  are measured in terms of  $\ell$ ,  $L$ ,  $\tau$ , and the density  $\rho$ , with the units  $\rho L^2/\tau^2$ ,  $\ell/\tau$ , and  $L/\tau$ , respectively. Additionally,  $\mu/\rho$  is implicitly related to  $L$  and  $\tau$  as  $\tau \sim L^2\rho/\mu$ . Given the radial  $\mathbf{e}_r$  and longitudinal  $\mathbf{e}_z$  cylindrical unit vectors, we radially expand in the bulk [ $r < h(z, t)$ ] the dimensionless pressure  $p(r, z, t)$  and the velocity fields  $\mathbf{v}(r, z, t) = u(r, z, t)\mathbf{e}_r + v(r, z, t)\mathbf{e}_z$  by using the aforementioned parameter  $\epsilon = \ell/L \ll 1$ ; below we link with the finite interface as a matching condition in terms of its thickness  $\delta$  and mobility  $M$  from the Cahn-Hilliard description.

We next take advantage of these previous standard ideas by the classical variable expansion,

$$p(r, z, t) = p_0(z, t) + p_2(z, t)(\epsilon r)^2 + \dots, \quad (2a)$$

$$v(r, z, t) = v_0(z, t) + v_2(z, t)(\epsilon r)^2 + \dots, \quad (2b)$$

$$u(r, z, t) = -v_{0z}(z, t)\epsilon r/2 - v_{2z}(z, t)(\epsilon r)^3/4 + \dots, \quad (2c)$$

which simultaneously satisfies mass conservation and the symmetry of the problem.

Once the Navier-Stokes equations are simplified with the variable expansion and after retaining the leading terms [1], the classical axial momentum equation is

$$v_{0r} + v_0 v_{0z} + p_{0z} = 4v_2 + v_{0zz}. \quad (3)$$

Both the bulk and the finite-thickness interface flow together through a quiescent outer fluid with a density  $\rho_o$  and a viscosity  $\mu_o$  that does not exert any external stress over the entire jet (Fig. 1). Thus, there is an inner balance of stresses between both domains through the boundary line that enables us to add the resulting net normal  $f^{(n)}$  and shear  $f^{(s)}$  stresses from the interface to the bulk at  $r = h(z, t)$ , leading to two dimensionless equations along the normal  $n$  and tangential  $s$  coordinates (see Fig. 1):

$$p - \frac{2[u_r + \epsilon^2 v_z h_z^2 - (v_r + \epsilon^2 u_z)h_z]}{1 + \epsilon^2 h_z^2} = f^{(n)}, \quad (4a)$$

$$\frac{2\epsilon^2 h_z(u_r - v_z) + (v_r + \epsilon^2 u_z)(1 - \epsilon^2 h_z^2)}{\epsilon(1 + \epsilon^2 h_z^2)} = \epsilon f^{(s)}. \quad (4b)$$

For the evaluation of  $f^{(n)}$  and  $f^{(s)}$  we utilize the Cahn-Hilliard formulation [16–18] for the fluid fraction  $\phi$ , which is based on the behavior of the chemical potential  $\theta = \phi^3 - \phi - \delta^2 \nabla^2 \phi$  that is formed by the competition between the phase separation,  $\phi^3 - \phi$ , and interface penalizing,  $-\delta^2 \nabla^2 \phi$ , terms:

$$\phi_t + (\mathbf{v}^{(i)} - \mathbf{v}^{(s)}) \cdot \nabla \phi = \frac{3M\sigma}{2\sqrt{2}\delta} \nabla^2 (\phi^3 - \phi - \delta^2 \nabla^2 \phi). \quad (5)$$

The difference of velocity components along  $n$  and  $s$ , respectively, from the inner interface  $\mathbf{v}^{(i)} = u^{(i)}\mathbf{n} + v^{(i)}\mathbf{s}$  to the boundary streamline  $\mathbf{v}^{(s)} = u^{(s)}\mathbf{n} + v^{(s)}\mathbf{s}$ , is assumed to be of  $O(\epsilon)$  due to the departures of the interface from a sort of frozen state. Next, we take advantage of the slenderness of the interface as  $\delta \sim \ell \ll L$  and  $\partial/\partial s \sim 1/L \ll \partial/\partial n \sim 1/\delta \sim 1/\ell$ . Thus, we neglect shear derivatives for terms that involve  $\nabla \phi$  (i.e.,  $\nabla \approx \mathbf{n}\partial/\partial n$ ). In addition, our expansion parameter can be scaled as  $\epsilon \sim (3M\rho/2\sqrt{2}\tau)^{1/2}$  in order to enable compatibility of capillary waves along with the interface [18] as  $\phi_t$  cannot be neglected. This scaling for  $\epsilon$  should be seen as an equivalent squared Cahn number, also estimated in Ref. [18]. Subsequently, this matching condition comes from the spatiotemporal coupling between both the interface and the bulk within the earliest stages of this pinch-off regime after leaving the equilibrium. Thus, we can utilize the viscous-capillary dimensional group to express interfacial parameters, where  $\sigma/\ell \sim \rho L^2/\tau^2$ . Then,  $\phi(n, s, t)$  varies from the boundary line  $r = h(z, t)$  (where  $\phi = -1$ ) to the outer fluid ( $\phi = 1$ ). With these simplifications, Eq. (5) then relates the second-order derivative of the chemical potential to the temporal evolution of  $\phi$ :

$$\phi_t = (\phi^3 - \phi - \phi_{nn})_{nn}. \quad (6)$$

The reader should notice that  $\delta$  is not present in the previous equation and hereafter as a result of our aforementioned simplifications and strategy of nondimensionalization. In this way, the chemical potential  $\theta$  turns out to be  $\theta = \phi^3 - \phi - \phi_{nn}$ .

We are interested in the expressions of the resulting net stresses across the interface,  $f^{(n)}$  and  $f^{(s)}$ , which result from the momentum equations due to the  $\phi$ -phase variations. This identification

is realistic as we focus on a liquid jet flowing through a quiescent surrounding medium with a low-viscosity  $\mu_o$  as  $\mu \gg \mu_o$  and without any extra external force over the whole fluid system (i.e., finite interface and bulk). First, we write the coupled set of nondimensional Cahn-Hilliard Navier-Stokes momentum equations, retaining each side's dominant contribution [18], as

$$u_t^{(i)} + \epsilon(u^{(i)} - u^{(s)})u_n^{(i)} + \epsilon(v^{(i)} - v^{(s)})u_s^{(i)} + \frac{\rho p_n}{\rho_i} - \frac{\rho \mu_i u_{nn}}{\rho_i \mu} = -\frac{3\rho \kappa \phi_n^2}{2\sqrt{2}\rho_i}, \quad (7a)$$

$$v_t^{(i)} + \epsilon(u^{(i)} - u^{(s)})v_n^{(i)} + \epsilon(v^{(i)} - v^{(s)})v_s^{(i)} + \frac{\rho p_s}{\rho_i} - \frac{\rho \mu_i v_{nn}}{\epsilon^2 \rho_i \mu} = \frac{3\rho \theta \phi_s}{2\sqrt{2}\rho_i}, \quad (7b)$$

where  $\rho_i$ ,  $\mu_i$ , and  $\kappa = 1/h + O(\epsilon^2)$  are the inner density, the viscosity of the interface, and its first-order curvature, respectively, where  $\mu_i$  is classically assumed to vary linearly with  $\phi$ . Note that we take advantage of our previous scaling where  $\epsilon$  and the squared Cahn number are linked. The interface's slenderness also leads to having a dominant shear speed component (i.e., this statement can be better understood if we think in absolute coordinates) as we have  $u^{(s)} = 0$  at both the liquid-interface boundary line and the outer streamline between the interface and the environment. From the integration of Eqs. (7) along the normal direction as analogously was performed for a single outer length scale by Magaletti and coworkers [18], we obtain the first-order expressions of  $f^{(n)}$  and  $f^{(s)}$ , being stresses that are ultimately transferred to the bulk through the boundary line in Eqs. (4):

$$f^{(n)} = \Delta(p_n) = \frac{3\kappa}{2\sqrt{2}} \int_0^\delta \phi_n^2 dn, \quad (8a)$$

$$\epsilon f^{(s)} = -\Delta(v_{nn}) = \frac{3\epsilon^2 \mu}{2\sqrt{2}} \int_0^\delta \frac{\theta \phi_s}{\mu_i} dn. \quad (8b)$$

We observe that the classical balances at the interface  $f^{(n)} = \kappa$  and  $f^{(s)} = 0$  are special cases of our more general approach towards an infinitely-narrow interface where  $\phi^{ss} = \tanh(n/\sqrt{2})$  is the solution for the steady version of Eq. (6). In contrast, as we depart from the tanh solution, we have a  $\phi$ -dependent Laplace-Young expression and a nonzero, but much weaker than the latter,  $O(\epsilon^2)$  shear stress in Eq. (8). Now we substitute the set of radially expanded variables of the bulk, Eq. (2) into Eq. (4), leading to the bulk-interface boundary equations in terms of stresses along normal and shear coordinates, respectively:

$$p_{0z} + v_{0z} = f^{(n)}, \quad (9a)$$

$$-3v_{0z}h_z - v_{0zz}h + 2v_2h = f^{(s)}. \quad (9b)$$

We substitute the variable expansion from Eq. (2) into the equation of motion for the streamline of the bulk boundary  $h_t + v h_z = u$  along with the expressions for  $p_z$  and  $v_2$  from Eqs. (9) and  $f^{(n)}$  and  $f^{(s)}$  from Eqs. (8). Subsequently, from the evaluation of Eq. (3), we find a slender model for the liquid jet at the scale of the interface:

$$h_t + v_0 h_z = -\frac{1}{2} v_{0z} h, \quad (10a)$$

$$v_{0t} + v_0 v_{0z} = \frac{3(v_{0z} h^2)_z}{h^2} + \frac{3}{2\sqrt{2}} \frac{h_z}{h^2} \int \phi_n^2 dn + \frac{3\epsilon \mu}{2\sqrt{2}h} \int \frac{\theta \phi_s}{\mu_i} dn + v_{0zz}, \quad (10b)$$

which corresponds to two equations for the unknowns  $h(z, t)$  and  $v_0(z, t)$  and a parametric dependence on  $\phi(n, s, t)$  because  $\phi_t \neq 0$  in Eq. (6). Note how the second, third, and fourth terms on the right-hand side of Eq. (10b) respectively correspond to a diffusive surface tension stress, a nonzero interface shear stress, and the retainment of  $v_{0zz}$  from the classical expansion where it is systematically neglected. Indeed, this extra term  $v_{0zz}$  appears as we relax the zero free-shear stress boundary conditions of the classical slender model [19] towards a subdominant role in our formulation. The reader should notice how the set of the derived governing equations, although

corresponding to two well-defined and separated regions of the fluid domain, are inherently linked through a spatiotemporal coupling within the pinching of the whole fluid system as the temporal dependence of  $\phi$  creates a transient dynamics that prevents the stability of the classical steady-state solution in the finite-thickness interface.

*Towards the singularity.* Next, we seek the physical behavior of Eqs. (10) close to the pinch-off. For this reason, we take  $t^* = t_b - t$  and  $z^* = z - z_b$  as the time  $t^*$  and length  $z^*$  scales before the breakup. As  $t^*, z^* \rightarrow 0$ , the change of variables

$$\xi = t^{*-1/2} z^*, \quad (11a)$$

$$\eta = t^{*-1/4} n, \quad (11b)$$

$$\phi = t^{*\chi} \Phi(\eta), \quad (11c)$$

$$h = t^{*(2\chi+3/4)} H(\xi), \quad (11d)$$

$$v_o = t^{*-1/2} V(\xi) \quad (11e)$$

enable us to balance the interface penalizing term with the temporal variation of  $\phi$  along with the dominance of the stresses with origin in the diffusive surface tension over the interface shear contribution. Subsequently, both the bulk and the finite interface are spatiotemporally tied, and from Eqs. (6) and (10) we find similarity equations:

$$-\chi \Phi + \frac{\eta \Phi_\eta}{4} = -\Phi_{\eta\eta\eta}, \quad (12a)$$

$$-\left(2\chi + \frac{3}{4}\right)H + \frac{\xi H'}{2} = -\frac{1}{2}HV' - VH', \quad (12b)$$

$$\frac{V}{2} + \frac{\xi V'}{2} = -VV' + 4V'' + \frac{6V'H'}{H} + \frac{3H'}{2\sqrt{2}H^2} \int \Phi_\eta^2 d\eta, \quad (12c)$$

where  $' = d/d\xi$ . The three ordinary differential equations (12) describe two subspaces: the interface with Eq. (12a), where  $\Phi$  depends on  $\eta$  and parametrically on  $\chi$ ; and the bulk with  $\xi$  as the independent variable in the Eqs. (12b) and (12c) that govern  $H$  and  $V$ , which are affected by the value of  $\chi$  through both the prefactor of  $H$  in Eq. (12b) and the resulting varying surface tension stress. From Eq. (12b), we observe

$$H' = H \frac{\left(2\chi + \frac{3}{4}\right) - \frac{V'}{2}}{V + \frac{\xi}{2}} \quad (13)$$

and, consequently, the existence of a certain value  $\xi_0$  that makes  $H$  singular unless we also impose analytical properties to require  $V_1 = V'(\xi_0) = (4\chi + 3/2)$ .

*Results.* We construct a solution around  $\xi_0$  as a Taylor series expansion for  $H = \sum_{i=0}^{\infty} H_i(\xi - \xi_0)^i$  and  $V = \sum_{i=0}^{\infty} V_i(\xi - \xi_0)^i$ . Substituting them into Eqs. (12b) and (12c) and after algebraic manipulations, we obtain the terms of order  $\xi^1$  and  $\xi^2$  for  $H$  and  $V$ , respectively,

$$H_1 = \frac{9\xi_0 H_0^2}{H_0(9 - 8\chi) + \frac{3}{2\sqrt{2}}N}, \quad (14a)$$

$$V_2 = \frac{9\xi_0 H_0(3 - 4\chi)}{H_0(9 - 8\chi) + \frac{3}{2\sqrt{2}}N}, \quad (14b)$$

where  $N = \int \Phi_\eta^2 d\eta$ . Note that Eqs. (14) only depends on  $\xi_0$ ,  $H_0$ , and  $N$ , which are to be determined later. In addition, we derive a set of boundary conditions where the solution has to match the outer spatiotemporal scale at  $\eta, \xi \rightarrow \pm\infty$ , making the left-hand terms of Eqs. (12) vanish due to their slow temporal origin and leading to the asymptotic behaviors  $\Phi \propto \eta^{4\chi}$ ,  $H \propto \xi^{(4\chi + \frac{3}{2})}$ , and  $V \propto \xi^{-1}$ .

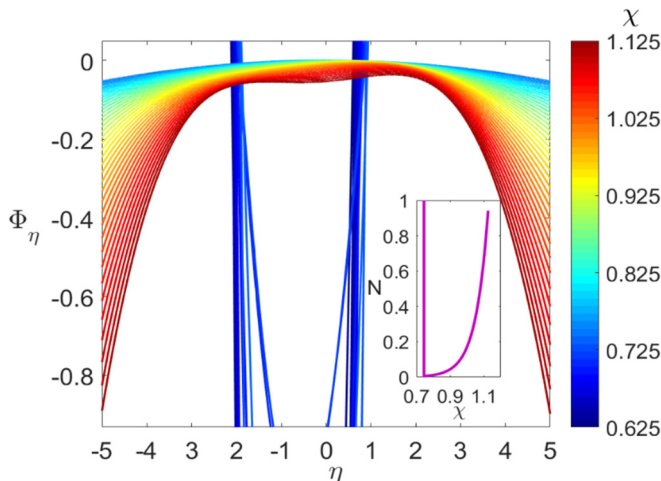


FIG. 2. Inner interfacial solutions of  $\Phi_\eta$  for  $\chi \in [0.625, 1.125]$ . The inset shows the relation between  $N$  and  $\chi$ , with a divergent behavior of  $N$  for  $\chi < \chi_{\min} = 0.745$  that corresponds to quasisymmetrical blue curves in the main figure.

On the one hand, the family of solutions of Eqs. (12) within the interface is numerically obtained (Fig. 2) by the shooting method for the derived boundary conditions, where the values  $N = 2\sqrt{2}/3$  and  $\chi = 9/8$  set the domain that recovers the unity prefactor of the surface tension stress term in the classical IV's momentum equation. It is also interesting to note that the length of the self-similar domain in  $\eta$  is not infinite in a strict sense and has a width of 15.6 (i.e., which was determined by machine-learning-based numerical strategies) to ensure both odd symmetry and only one inflexion point as the initial conditions from the base state solution impose when this pinch-off regime is triggered. However, this is far away enough to consider it as an approximation to ensure convergence to apply the aforementioned asymptotic boundary condition, with inspiration in classical works [5]. Then, we compute the resulting  $N$  by varying the value of  $\chi$  in Eq. (12a). We observe that the morphology of the solution varies abruptly (Fig. 2) as  $\chi < \chi_{\min} \approx 0.745$ , where  $N$  diverges. Indeed, the latter cases entail that interfacial velocities would reach infinite values that could not match the basic physical assumptions of the thinning jet and, consequently, are disregarded. We only consider the  $N - \chi$  curve for  $\chi > \chi_{\min}$ . Now, we seek a pair  $(\chi, N)$  that could lead to solutions of Eqs. (12b) and (12c) that exhibit symmetry with respect to  $\chi$  for the profiles of  $H$  and  $V$ , where we recall the same flow feature that on average takes place at the nanoscale [9] and also in larger-scaled pure diffusive experiments [12]. This strategy involves two parameters  $(\chi, N)$  tied to the thermal interface roughening and the diffusive pinch-off, respectively, as the breakup radius and speed profiles turn out to be symmetric in the self-similar space of  $\chi$ . We select the pair  $(\chi, N)$  that is compatible with the latter features. To do so, we numerically solve Eqs. (12b) and (12c) by the shooting method. For each  $(\chi, N)$ , first we assume the values  $(\xi_0, H_0)$  to evaluate the starting integration points for the branches of the solution on the right and left from  $\xi_0$ , by the expansion mentioned earlier [Eqs. (14)]. Then we obtain a curve of candidate values of  $(\xi_0, H_0)$  for both branches that are compatible with the defined boundary conditions for  $|\xi| \gg |\xi_0|$ .

The global solution for a given pair  $(\chi, N)$  is determined as both branches share the same location of the singularity  $\xi_0^*$  and its corresponding minimum thickness,  $H_0^*$ . In these solutions, we check the intended symmetric profiles as a function of  $\chi$  and its corresponding value of  $N$ . In particular, we observe in Fig. 3 how  $H$  profiles become more symmetric as  $\chi$  decreases. In addition, the smaller the value of  $\chi$  is, the smaller the minimum value of  $H$  is, and the closer  $\xi_0$  is to 0. Similar features occur with the respective  $V$  profiles shown in Fig. 4, although in this case the approach to symmetry is for an odd function instead of an even function. As  $\chi$  decreases,  $V$  profiles rotate

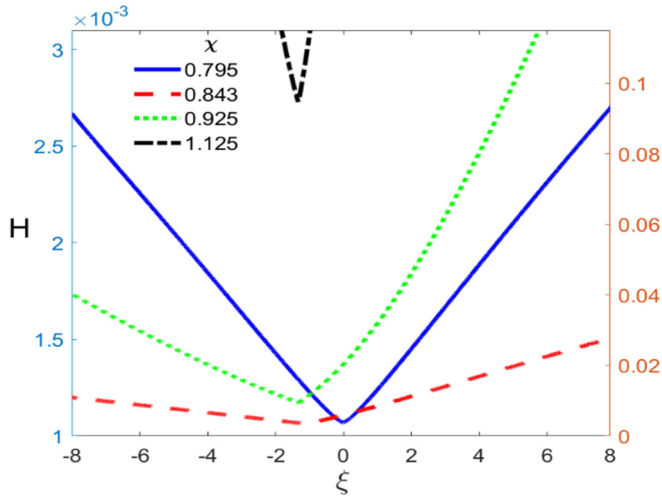


FIG. 3. Family of self-similar solutions for  $H$  as a function of  $\chi$ . There is only an even symmetric profile (blue, solid line) for  $\chi = 0.795$  (left vertical axis). The rest of the candidate curves are examples of how the symmetry is broken as  $\chi$  varies (right vertical axis).

clockwise as the singularity tends to move to 0. Ultimately, we find that the values  $\chi = 0.795$ ,  $N = 0.00953$ , and  $2\chi + 3/4 \sim 2.34$  lead to symmetric self-similar solutions for  $H$  and  $V$ , even and odd, respectively, along with  $\xi_0 = -0.01$  and  $H_0 = 0.00107$ . Hence, we arrive at an expression of the evolution of the minimum neck radius  $h_{\min} = 0.00107(t_b - t)^{2.34}$ . Thus, we have solved an open fundamental problem and provided keys for approaching a vast number of fluid phenomena that involve topological changes close to the continuum limit.

*Prospects.* Using the approach presented in this paper, it should be possible to address other open questions in jet-related fundamental problems:

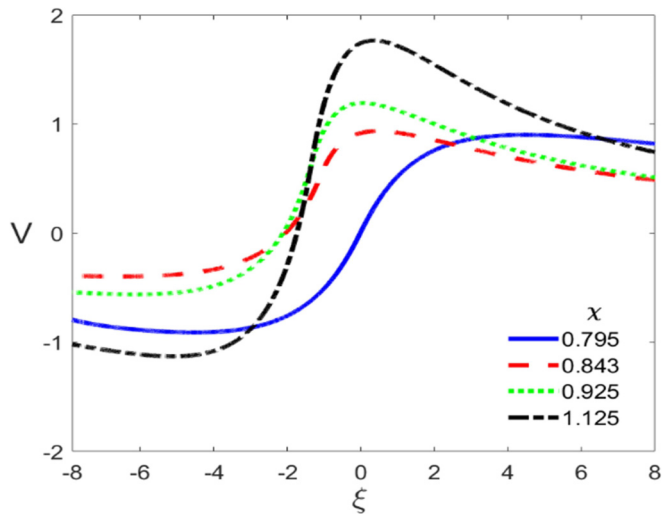


FIG. 4. Family of self-similar solutions for  $V$  as a function of  $\chi$ . There is only an odd symmetric profile (blue solid line) for  $\chi = 0.795$ . The rest of the candidate curves are examples of how the symmetry is broken as  $\chi$  varies.



- (i) the relation between the intact jet length and its instability [20], with a self-destabilizing loop close to the breakup region [21], to better appreciate the role played by transient pinch-off regimes;
- (ii) the relation between pinch-off and recoil dynamics with the absence of satellite droplets in pure diffusive experiments [12,13];
- (iii) the role of interfacial fluctuations close to the continuum limit [9,10] and whether or not they emerge before those that come from the bulk and, if so, how both energetic levels might compete within the fragmentation; and
- (iv) the extension of this work, together with the above points, to widely studied coflowing streams [22–29] or electrosprays [30–34], where, probably below a specific scale, the finiteness of the Debye layer and diverse electrokinetic effects might appear [35].

F.C.-M. acknowledges that this project has received funding from the European Union’s Horizon 2020 research and innovation programme under the Marie Skłodowska-Curie Grant No 838997. We thank the NSF for support via Grant No. CBET-1804863.

- 
- [1] J. Eggers and E. Villermaux, Physics of liquid jets, *Rep. Prog. Phys.* **71**, 036601 (2008).
  - [2] Z. Takáts, J. M. Wiseman, B. Gologan, and R. G. Cooks, Mass spectrometry sampling under ambient conditions with desorption electrospray ionization, *Science* **306**, 471 (2004).
  - [3] H. N. Chapman *et al.*, Femtosecond x-ray protein nanocrystallography, *Nature (London)* **470**, 73 (2011).
  - [4] M. Gamero-Castaño and V. Hruby, Electrospray as a source of nanoparticles for efficient colloid thrusters, *J. Propul. Power* **17**, 977 (2001).
  - [5] J. Eggers, Universal Pinching of 3D Axisymmetric Free-Surface Flow, *Phys. Rev. Lett.* **71**, 3458 (1993).
  - [6] J. R. Castrejón-Pita, A. A. Castrejón-Pita, S. S. Thete, K. Sambath, I. M. Hutchings, J. Hinch, J. R. Lister, and O. A. Basaran, Plethora of transitions during breakup of liquid filaments, *Proc. Natl. Acad. Sci. USA* **112**, 4582 (2015).
  - [7] Y. Li and J. E. Sprittles, Capillary breakup of a liquid bridge: identifying regimes and transitions, *J. Fluid Mech.* **797**, 29 (2016).
  - [8] A. Deblais, M. A. Herrada, I. Hauner, K. P. Velikov, T. van Roon, H. Kellay, J. Eggers, and D. Bonn, Viscous Effects on Inertial Drop Formation, *Phys. Rev. Lett.* **121**, 254501 (2018).
  - [9] M. Moseler and U. Landman, Formation, stability, and breakup of nanojets, *Science* **289**, 1165 (2000).
  - [10] J. Eggers, Dynamics of Liquid Nanojets, *Phys. Rev. Lett.* **89**, 084502 (2002).
  - [11] W. Kang and U. Landman, Universality Crossover of the Pinch-Off Shape Profiles of Collapsing Liquid Nanobridges in Vacuum and Gaseous Environments, *Phys. Rev. Lett.* **98**, 064504 (2007).
  - [12] Y. Hennequin, D. G. A. L. Aarts, J. H. van der Wiel, G. Wegdam, J. Eggers, H. N. W. Lekkerkerker, and D. Bonn, Drop Formation by Thermal Fluctuations at an Ultralow Surface Tension, *Phys. Rev. Lett.* **97**, 244502 (2006).
  - [13] J. Petit, D. Rivière, H. Kellay, and J. Delville, Break-up dynamics of fluctuating liquid threads, *Proc. Natl. Acad. Sci. USA* **109**, 18327 (2012).
  - [14] H. Y. Lo, Y. Liu, S. Y. Mak, Z. Xu, Y. Chao, K. J. Li, H. C. Shum, and L. Xu, Diffusion-Dominated Pinch-Off of Ultralow Surface Tension Fluids, *Phys. Rev. Lett.* **123**, 134501 (2019).
  - [15] C. Zhao, D. A. Lockerby, and J. E. Sprittles, Dynamics of liquid nanothreads: Fluctuation-driven instability and rupture, *Phys. Rev. Fluids* **5**, 044201 (2020).
  - [16] J. W. Cahn and J.E. Hilliard, Free energy of a nonuniform system. I. Interface free energy, *J. Chem. Phys.* **28**, 258 (1958).
  - [17] J. Lowengrub and L. Truskinovsky, Quasi-incompressible Cahn-Hilliard fluids and topological transitions, *Proc. R. Soc. London, Ser. A* **454**, 2617 (1998).
  - [18] F. Magaletti, F. Picano, M. Chinappi, L. Marino, and C. M. Casciola, The sharp-interface limit of the Cahn-Hilliard/Navier-Stokes model for binary fluids, *J. Fluid Mech.* **714**, 95 (2013).



- [19] J. Eggers and T. F. Dupont, Drop formation in a one-dimensional approximation of the Navier-Stokes equation, *J. Fluid Mech.* **262**, 205 (1994).
- [20] S. Le Dizés and E. Villermaux, Capillary jet breakup by noise amplification, *J. Fluid Mech.* **810**, 281 (2017).
- [21] A. Umemura, Self-destabilising loop of a low-speed water jet emanating from an orifice in microgravity, *J. Fluid Mech.* **797**, 146 (2016).
- [22] J. R. Lister, Selective withdrawal from a viscous two-layer system, *J. Fluid Mech.* **198**, 231 (1989).
- [23] A. M. Gañán-Calvo, Generation of Steady Liquid Microthreads and Micron-Sized Monodisperse Sprays in Gas Streams, *Phys. Rev. Lett.* **80**, 285 (1998).
- [24] I. Cohen, H. Li, J. L. Houglund, M. Mrksich, and S. R. Nagel, Using selective withdrawal to coat microparticles, *Science* **292**, 265 (2001).
- [25] S. L. Anna, N. Bontoux, and H. A. Stone, Formation of dispersions using flow focusing in microchannels, *Appl. Phys. Lett.* **82**, 364 (2003).
- [26] A. S. Utada, E. Lorenceau, D. R. Link, P. D. Kaplan, H. A. Stone, and D. A. Weitz, Monodisperse emulsions generated from a microcapillary device, *Science* **308**, 537 (2005).
- [27] A. S. Utada, A. Fernandez-Nieves, H. A. Stone, and D. A. Weitz, Dripping to Jetting Transitions in Coflowing Liquid Streams, *Phys. Rev. Lett.* **99**, 094502 (2007).
- [28] F. Cruz-Mazo, J. M. Montanero, and A. M. Gañán-Calvo, Monosized dripping mode of axisymmetric flow focusing, *Phys. Rev. E* **94**, 053122 (2016).
- [29] A. Dewandre, J. Rivero-Rodriguez, Y. Vitry, B. Sobac, and B. Scheid, Microfluidic droplet generation based on non-embedded co-flow-focusing using 3D printed nozzle, *Sci. Rep.* **10**, 21616 (2020).
- [30] G. Taylor, Disintegration of water drops in electric field, *Proc. R. Soc. London A* **280**, 383 (1964).
- [31] I. G. Loscertales, A. Barrero, I. Guerrero, R. Cortijo, M. Marquez, and A. M. Gañán-Calvo, Micro/nano encapsulation via electrified coaxial liquid jets, *Science* **295**, 1695 (2002).
- [32] A. M. Gañán-Calvo, J. M. López-Herrera, and P. Riesco-Chueca, The combination of electrospray and flow focusing, *J. Fluid Mech.* **566**, 421 (2006).
- [33] R. T. Collins, K. Sambath, M. T. Harris, and O. A. Basaran, Universal scaling laws for the disintegration of electrified drops, *Proc. Natl. Acad. Sci. USA* **110**, 4905 (2013).
- [34] F. Cruz-Mazo, M. O. Wiedorn, M. A. Herrada, S. Bajt, H. N. Chapman, and A. M. Gañán-Calvo, Aerodynamically stabilized Taylor cone jets, *Phys. Rev. E* **100**, 031101(R) (2019).
- [35] A. Gupta, P. J. Zuk, and H. A. Stone, Charging Dynamics of Overlapping Double Layers in a Cylindrical Nanopore, *Phys. Rev. Lett.* **125**, 076001 (2020).